Advanced subsea imaging technique of digital holography: in situ measurement of marine microscale plankton and particles

Zonghua Liu [1,2,*], Sarah Giering[1], Tomoko Takahashi[3], Thangavel Thevar[4], Marika Takeuchi[1], Nick Burns[5], Blair Thornton[2,6], John Watson[4], and Dhugal Linsday[3]

[1] National Oceanography Centre, Southampton, UK
[2] IIS, University of Tokyo, Tokyo, Japan
[3] JAMSTEC, Yokosuka, Kanagawa, Japan
[4] School of Engineering, University of Aberdeen, Aberdeen, UK
[5] Hi-Z 3D LTD, London, UK
[6] Faculty of Engineering and Physical Sciences, University of Southampton, Southampton, UK

***Abstract*—Studying the amount, variety, and distribution of microscale particles and plankton at the global scale at different times and seasons is very important to understand ocean environments, and by reference, the global environment. It is important to image them in their natural habitats. Many optical techniques have been developed to meet this requirement. Most techniques suffer from one or another drawbacks, such as limited depth-of-field or low volume. Digital holography is an advanced optical imaging technique to image micro-objects, and it provides high-resolution recording, large depth-of-field and recording volume, and 3D viewing and tracking. This paper describes basic principles of in-line digital holography and provides common image processing methods. Four submersible digital holographic cameras, eHoloCam, RamaCam, weeHoloCam, and LISST-Holo, are introduced, as well as their image processing software. At the end, some limitations and challenges in the underwater holographic imaging systems are mentioned, and some possible solutions are discussed.**

***Index Terms*—digital holography, submersible holographic cameras, marine microscale particles and plankton, hologram processing**

I. Introduction

The importance of microscale particles and plankton in oceans has been recognised by the Global Ocean Observing System [1]. They, including live plankton, organic sediments (e.g. marine snow), and inorganic particulate matter, play a crucial role in the oceanic environments and for global biogeochemical cycles. Marine scientists have estimated that oceanic plankton is responsible for 50 – 80% of the oxygen production on Earth [2]. Large amounts of carbon dioxide (5 – 15 gigatonnes per year [3]) are also stored in the deep ocean via sinking particles. Besides these ecosystem services, the foundation of the marine food chain is marine phytoplankton [4]. In the current decades, due to human activities, massive quantities of micro-plastics are now suspended in vast areas of the oceans across the world. They have caused serious pollution in the oceans and are damaging the ocean ecosystem. Therefore, measuring and monitoring abundance, variety and distribution at a global scale at different times and seasons is critical to understand the oceanic ecosystems and predict its future in a changing world.

It is important to image marine particles in their natural habitats, that is, in the field. Many optical systems have been developed to meet this requirement, and different techniques were used. Some researchers developed underwater microscopes, e.g. CPICS [5], and they are capable of recording high-resolution images of marine objects at the scale down to 10 micrometres. However, they suffer a reduction in field of view due to the used objective lenses (0.3 mL in CIPICS). The technique of shadowgraphy allows to image meso-plankton/particles in larger sampling volumes (˜240 mL in ZOOVIS [6]). Another similar technique that allows large imaging volumes uses reflected or scattered light from particles (˜700 mL in UVP6 [7]). But these two techniques generally cannot provide fine high-resolution images to microscale targets ($<$100 μm).

Holography is an advanced optical imaging technique which can be used to image microscale objects in large depth-of-field. This technique is different from other traditional optical imaging techniques, and it is based on optical interference and diffraction. Compared with other techniques, as well as high-resolution and large-volume recording (based on the structure [8, 9]), it also provides 3D viewing and tracking to particles. Sophisticated and small-size hardware, such as lasers and imaging sensors, accelerates the development of compact and powerful underwater digital holographic cameras (holocameras), and facilitates the application of digital holography (DH) to in situ measurements of marine microscale plankton and particles.

This paper introduces the application history of holography in marine sciences, and four submersible holocameras, eHoloCam, RamaCam, weeHoloCam, and LISST-Holo, that we used

* zonghua.liu@noc.ac.uk

or developed in research. Some images recorded by them are shown, and some data analysis based on the collected images is given as well. Some limitations and challenges in the underwater holographic imaging systems are mentioned. At the end, some possible solutions to those challenges and popular research topics related to applications of digital holography in oceans are discussed.

II. Holography and History

In optical holography (in this paper, holography means the optical holography), the source is coherent laser waves. A wave illuminates on a target, as shown in Fig. 1-(a). The scattered wave from the target surface, referred to as the object wave $E_O(x,y)$, interferes with the reference wave $E_R(x,y)$ which directly illuminates the plate, and this produces the interference pattern on the plate. The pattern is the hologram. The intensity on the recording medium (normally a plate or film, in classical holography) can be described as:

$$\begin{aligned} I(x,y) &= |E_O(x,y) + E_R(x,y)|^2 \\ &= |a_O(x,y)\exp(i\varphi_O(x,y)) + a_R(x,y)\exp(i\varphi_R(x,y))|^2 \\ &= a_O^2 + a_R^2 + a_O a_R \exp(i\varphi_{OR}) + a_O a_R \exp(i(\varphi_{RO})), \end{aligned} \tag{1}$$

where $a(x,y)$ and $\exp(i\varphi(x,y))$ indicate the amplitude and phase respectively; $\varphi_{OR} = \varphi_O - \varphi_R$ and $\varphi_{RO} = \varphi_R - \varphi_O$.

The amplitude transmission $h(x,y)$ of a hologram is proportional to its intensity, and can be described as $h(x,y) = \tau I(x,y)$. When reconstructing a hologram, the hologram is illuminated using the same wave with the reference wave (see Fig. 1-(b)), and the reconstructed wavefront is:

$$\begin{aligned} E_{rec}(x,y) &= E_R(x,y)h(x,y) \\ &= \tau(a_O^2 + a_R^2)E_R(x,y) + \tau a_R^2 E_O + \tau E_R^2 E_O^*, \end{aligned} \tag{2}$$

where E_O^* is conjugated E_O. In the above equation, the first term represents the non-diffracted wave (DC term), the second and third terms respectively form the virtual and real images of the target.

While holograms are recorded on photosensitive mediums in classical holography, they are recorded on electronic sensors (e.g. CCD or CMOS sensors) in DH. When recording a hologram, either the plane wave (collimated) or spherical wave (point-source) can be used as the incident wave to illuminate a target. If the incident wave propagates along the same optical axis as the reference wave, this is called in-line recording; if they have different optical axes, this is called off-axis recording. Most DH systems adopt the in-line recording configuration with the plane incident wave, as shown in Fig. 1-(a), because this structure is simple and compact, and corresponding hologram processing is easy as well. Therefore, this paper mainly focusses on digital in-line holography with the plane wave. This structure allows large-volume recording (see TABLE I).

The history of holography can be tracked back to 1940's when Dennis Gabor invented holography with X-Ray [10]. In

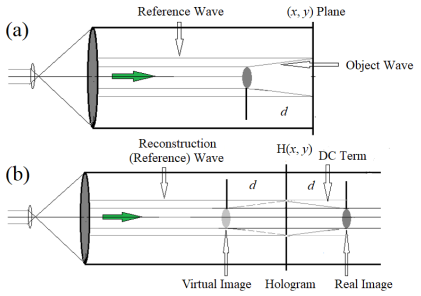

Fig. 1. In-line hologram recording using the plane wave (a), and the process of hologram reconstruction (b).

1966, Knox first used laser holography for plankton research [11]. He built up an in-line setup in the laboratory and used it to image plankton onto chemical films. The first reported in situ underwater holocamera was developed by Stewart's group in 1973 [12]. This camera was deployed within the upper 100 m underwater and imaged marine plankton onto in-line holograms. Heflinger and his colleagues developed a high-resolution off-axis holocamera to study rapidly moving marine zooplankton in 1978 [13]. Afterwards, several groups contributed to developing and applying submersible holocameras to measure the abundance, distribution, sizes, and characteristics and motions of oceanic particulates, including the work published by Carder et al. in 1982 [14], Payne et al. in 1984 [15], O'Hern et al. in 1988 [16], Watson et al. in 1995 [17]. A remotely operated submersible holocamera was reported by Katz et al. in 1999 [18]. This instrument was configured for in-line holography, but it could be modified into the off-axis configuration. Another representative in situ holographic system able to record in-line and off-axis holograms is HoloCam demonstrated by Watson et al. in 2001 [19].

Although classical holocameras offer holograms of large sampling volumes at high resolutions, a mechanical system is needed to change films, and it is also time consuming to process the recorded films. Their bulky and heavy bodies also prevent them from easy deployments at sea. Technological advancements in high-resolution digital sensors facilitated the emergence of DH. In 2000, Owen and his colleague [20] first reported their work on monitoring marine plankton using an in situ digital holographic system. Thereafter, lightweight and compact digital holocameras started to be the mainstream for in situ sampling marine plankton and particles with holography.

In 2005, Fitsch et al. reported a free-drifting submersible digital holographic imaging system [21]. This camera records two in-line holograms from orthogonal directions which not only increases the sampling volume and also provides dual views of targets. One year later, Jericho et al. [22] developed a simple digital in-line holographic microscope (DIHM) using a point-source of light. This instrument was designed for a depth of 20 m underwater, and was able to record marine organisms and their motions with micron resolution. Sun et al. in 2007 published a paper to describe an in situ underwater

electronic holocamera (eHoloCam) [9] developed to study the distribution and dynamics of marine organisms and particles. The camera was designed to dive up to 3000 m and was pressure-tested and certified to 1800 m. Graham et al. in 2010 [23], developed an in situ digital in-line holocamera to estimate size distributions and settling velocities of suspended cohesive sediments. In 2013, a digital DIHM developed by Bochdansky et al. was reported [24], and it was the first holocamera that was deployed to 6000 m water depth. Nayak et al. in 2018 reported a submersible holocamera (HOLOCAM) [25]. This system can be operated in a lens-less configuration as well as with a microscopic objective. In 2020, they reported an novel, in situ, autonomous holocamera named AUTOHOLO [26], and it is untethered and battery-powered. Dyomin et al. developed a series of very large sampling-volume holocameras [27-29] with a single imaging sensor. A common highlight of these cameras is that a mirror-prism system is used to significantly increase the recording volume. A representative camera can record a 750 mL water valume [29]. Thevar et al. developed a very compact in-line holocamera (weeHoloCam) in 2021 [30]. Two commercial systems LIIST-HOLO [31] and HoloSea [32] are also available. TABLE I gives more information on some selected in-line holocameras.

III. Hologram Processing

This paper focuses on in-line hologram (recorded with the plane wave) processing. To reveal the morphological property of a recorded object in a hologram, its hologram needs to be first reconstructed at its recording distance. This process mainly consists of two steps: hologram reconstruction and focusing. Since much noise exists in holograms, some methods have been developed to suppress noise before or during reconstruction.

A. Reconstruction

In the classical holography, a laser wave identical to the reference wave ($E_R(x,y)$) used in the process of recording is used to illuminate the hologram ($h(x,y)$), as shown in Fig. 1-(b). Based on the Fresnel-Kirchhoff diffraction integral, the reconstruction of a hologram can be described by back-propagation of the reference wave through the hologram plane (x,y) to a reconstruction plane (ξ,η) as:

$$E(\xi,\eta)=\frac{i}{\lambda}\iint_{-\infty}^{+\infty}E_R(x,y)h(x,y)\frac{\exp(-i\frac{2\pi}{\lambda}\rho)}{\rho}dxdy, \quad (3)$$

where $\rho=\sqrt{(x-\xi)^2+(y-\eta)^2+d^2}$ which describes the distance between a point in the hologram plane and a point in the reconstruction plane. The object image is formed at the position where the object was recording from the recording plane (the hologram plane).

In DH, this process can be simulated on a computer using a reconstruction algorithm. A plane wave can be described as $E_R = a_R\exp(i\vec{k}.\vec{r})$ with wave vector $\left|\vec{k}\right| = 2\pi/\lambda$. By selecting its propagation origin, direction, and intensity, $E_R(x,y)$ could be set as 1. Therefore, Eq. 3 can be simplified as:

$$\begin{aligned}&E(\xi,\eta)=\frac{i}{\lambda}\iint_{-\infty}^{+\infty}h(x,y)\times\\&\frac{\exp(-i\frac{2\pi}{\lambda}\sqrt{(x-\xi)^2+(y-\eta)^2+d^2}}{\sqrt{(x-\xi)^2+(y-\eta)^2+d^2}}dxdy.\end{aligned} \quad (4)$$

Several methods have been developed to numerically efficiently process this integral.

1) Near-field Fresnel approximation: When the object is recorded sufficiently far from the sensor plane such that Fresnel approximation

$$d\gg\sqrt[3]{\frac{1}{8}\frac{[(x-\xi)^2+(y-\eta)^2]^2}{\lambda}} \quad (5)$$

is fulfilled, ρ in the numerator of Eq. 4 approximates to $(x-\xi)^2/(2d)+(y-\eta)^2/(2d)+d$ which is calculated based on Taylor series expansion. Hence, Eq. 4 can be rewritten as

$$\begin{aligned}&E(\xi,\eta)=\frac{i}{\lambda d}\exp(-i\frac{2\pi}{\lambda}d)\times\\&\iint_{-\infty}^{+\infty}h(x,y)\exp\left\{-i\frac{\pi}{\lambda d}[(x-\xi)^2+(y-\eta)^2]\right\}dxdy\\&=\frac{i}{\lambda d}\exp(-i\frac{2\pi}{\lambda}d)\exp[-i\frac{\pi}{\lambda d}(\xi^2+\eta^2)]\times\\&\iint_{-\infty}^{+\infty}h(x,y)\exp[-i\frac{\pi}{\lambda d}(x^2+y^2)]\exp[-i\frac{2\pi}{\lambda d}(x\xi+y\eta)]dxdy.\end{aligned} \quad (6)$$

This equation is known as the Fresnel transform. It can be calculated using the inverse Fourier Transform with introducing $\mu=\xi/(\lambda d)$ and $\nu=\eta/(\lambda d)$ as:

$$\begin{aligned}&E(\mu,\nu)=\frac{i}{\lambda d}\exp(-i\frac{2\pi}{\lambda}d)\exp[-i\pi\lambda d(\mu^2+\nu^2]\times\\&\mathfrak{F}^{-1}\left\{h(x,y)\exp[-i\frac{\pi}{\lambda d}(x^2+y^2)]\right\},\end{aligned} \quad (7)$$

where $\mathfrak{F}^{-1}$ denotes the inverse Fourier transform.

If the sensor (hologram) has M × N pixels with steps $\triangle x$ and $\triangle y$, the Fresnel transform can be digitised as:

$$\begin{aligned}&E(m,n)=\frac{i}{\lambda d}\exp(-i\frac{2\pi}{\lambda}d)\times\\&\exp\left\{-i\pi\lambda d[(\frac{m}{\mathrm{M}\triangle\mathrm{x}})^2+(\frac{n}{\mathrm{N}\triangle\mathrm{y}})^2]\right\}\times\\&\mathfrak{F}^{-1}\left\{h(k,l)\exp[-i\frac{\pi}{\lambda d}[(k\triangle x)^2+(l\triangle y)^2)]\right\}.\end{aligned} \quad (8)$$

The intensity and phase on a reconstruction plane are given as

$$I(m,n)=|E(m,n)|^2;\phi(m,n)=\arctan\frac{Im(E(m,n))}{Re(E(m,n))}, \quad (9)$$

where Im and Re denote the real and imaginary parts of the reconstructed wave respectively.

TABLE I
SOME DIGITAL IN-LINE HOLOCAMERAS AND THEIR PARAMETERS LISTED BASED ON THE REPORT YEARS

In-line Systems	Laser		Sensor			Illuminating Light	Imaging Volume per Hologram (mL)	Max Depth (m)	Size (mm) (DxL; DxWxH)
	mode	wavelength (nm)	min pixel pitch (μm)	demision	max frame rate (fps)				
Holosub [21]	pulsed	660	7.4	2000×2000	15	collimated	2×40.5 (dual-view)	/*	/
DIHM in 2006 [22]	pulsed	532	6.4	1392×1040	7	point-source	0.009	20	/
eHoloCam in 2007 [9]	pulsed (4 ns)	532	3.5	2208×3000	25	collimated	36.5	3000	330×1350
system in 2010 [23]	CW	532	7.4	1002×1004	25	collimated	1.7	/	100×630
DIHM in 2013 [24]	CW	640	7.4	2048×2048	7	point-source	1.8	6000	150×890
HOLOCAM in 2018 [25]	/	660	4.59 (0.34)	2048×2048 (2432×2058)	15	collimated	3.53 (0.023)	/	/
AUTOHOLO in 2020 [26]	pulsed	532	4.59	4920×3280	3.5	collimated	71.4	/	/
DHC in 2022 [29]	pulsed	660	3.45	2464×2056	/	collimated	750	500	581×290.5 ×450
weeHoloCam in 2022 [30]	pulsed (3 ns)	532	3.45	2464×2056	20	collimated	12.1	500	90×600
LIIST-Holo2 [31]	CW	658	4.4	1600×1200	25	collimated	1.5	600	133×767
HoloSea S5 [32]	pulsed	386	7.4	2056×2060	22	point-source	0.063	2000	92×351

*There is no information found about this specification.

2) Far-field Fraunhofer approximation: If the object is recorded at a very large distance, the Fresnel approximation is replaced by the stronger Fraunhofer approximation: $d \gg (x^2+y^2)/(2\lambda)$. Eq. 7 hence converts into

$$E(\mu,\nu) = \frac{i}{\lambda d}\exp(-i\frac{2\pi}{\lambda}d)\exp[-i\pi\lambda d(\mu^2+\nu^2)]\times \mathfrak{F}^{-1}\left\{h(x,y)\right\}. \tag{10}$$

Now, the reconstructed object wave is just described by the inverse Fourier transform of the hologram transmission. Its discrete format is

$$E(m,n) = \frac{i}{\lambda d}\exp(-i\frac{2\pi}{\lambda}d)\times \exp\left\{-i\pi\lambda d[(\frac{m}{\mathrm{M}\triangle \mathrm{x}})^2+(\frac{n}{\mathrm{N}\triangle \mathrm{y}})^2]\right\}\mathfrak{F}^{-1}\left\{h(k,l)\right\}. \tag{11}$$

3) Convolution approach: The Fresnel-Kirchhoff diffraction integral can also be directly processed using the convolution theorem. Eq. 4 can be interpreted as

$$E(\xi,\eta) = \iint_{-\infty}^{+\infty} h(x,y)g(\xi-x,\eta-y)dxdy, \tag{12}$$

where $g(\xi-x,\eta-y) = \frac{i}{\lambda}\frac{\exp(-i\frac{2\pi}{\lambda}\sqrt{(x-\xi)^2+(y-\eta)^2+d^2})}{\sqrt{(x-\xi)^2+(y-\eta)^2+d^2}}$ can be regarded as an impulse response. This equation exactly describes the convolution of two functions of h and g. Based on the convolution theorem, Eq. 12 can be calculated as:

$$E(\xi,\eta) = \mathfrak{F}^{-1}\left\{\mathfrak{F}\{h\}\mathfrak{F}\{g\}\right\}, \tag{13}$$

where $\mathfrak{F}$ denotes the Fourier transform. The impulse response function g can be digitised by replacing the continuous differences $(x-\xi)$ and $(y-\eta)$ with the discrete variables $k\triangle x$ and $l\triangle y$ as $g(k,l) = \frac{i}{\lambda}\frac{\exp(-i\frac{2\pi}{\lambda}\sqrt{(k\triangle x)^2+(l\triangle y)^2+d^2})}{\sqrt{(k\triangle x)^2+(l\triangle y)^2+d^2}}$ with integer values $k = 0,1,\ldots,\mathrm{M}$ and $l = 0,1,\ldots,\mathrm{N}$. The Fourier transform of this expression can be analytically calculated as $G(m,n) = \exp\left\{-i\frac{2\pi d}{\lambda}\sqrt{1-(\frac{m\lambda}{\mathrm{M}\triangle \mathrm{x}})^2-(\frac{n\lambda}{\mathrm{N}\triangle \mathrm{y}})^2}\right\}$ [33] with integer values $m = 0,1,\ldots,\mathrm{M}$ and $n = 0,1,\ldots,\mathrm{N}$. Thus, Eq. 13 can now be rewritten as

$$E(\xi,\eta) = \mathfrak{F}^{-1}\left\{\mathfrak{F}\{h\}\exp\left\{-i\frac{2\pi d}{\lambda}\sqrt{1-(\frac{m\lambda}{\mathrm{M}\triangle \mathrm{x}})^2-(\frac{n\lambda}{\mathrm{N}\triangle \mathrm{y}})^2}\right\}\right\}. \tag{14}$$

4) Angular spectrum method: The angular spectrum is based on a theorem that a complex wave can be expanded into infinite plane waves with the same frequency and different propagation directions. Based on Fourier optics, the spectrum of the scattered wave on the hologram plan can be calculated by

$$\begin{aligned} A(k_x,k_y)|_{z=0} &= \mathfrak{F}\{h(x,y)\} \\ &= \iint_{-\infty}^{+\infty} h(x,y)\exp[-i(k_x x+k_y y)]dxdy \end{aligned} \tag{15}$$

where the direction vector $\vec{k} = (k_x,k_y,k_z) = \frac{2\pi}{\lambda}(\cos\varphi\sin\theta,\sin\varphi\sin\theta,\cos\theta)$. Set $\cos\varphi\sin\theta = \lambda\mu$ and $\sin\varphi\sin\theta = \lambda\nu$, and they fulfil $(\lambda\mu)^2+(\lambda\nu)^2 \le 1$. Thus, $k_z = \frac{2\pi}{\lambda}\sqrt{1-(\lambda\mu)^2-(\lambda\nu)^2}$. When the infinite plane waves propagate onto the plane $z = d$, their phases increase by $\exp(-k_z d)$, and the spectrum of the wave on this plane is described as

$$\begin{aligned} A(k_x,k_y)|_{z=d} &= \iint_{-\infty}^{+\infty} h(x,y)\exp[-i(k_x x+k_y y+k_z d)]dxdy \\ &= \mathfrak{F}\{h(x,y)\}\exp\left\{-i\frac{2\pi d}{\lambda}\sqrt{1-(\lambda\mu)^2-(\lambda\nu)^2}\right\}. \end{aligned} \tag{16}$$

Therefore, the wave on the reconstruction plane d is calculated by

$$E(\mu,\nu) = \mathfrak{F}^{-1}\{A(k_x,k_y)|_{z=d}\} = \mathfrak{F}^{-1}\left\{\mathfrak{F}\{h(x,y)\}\exp[-i\frac{2\pi d}{\lambda}\sqrt{1-(\lambda\mu)^2-(\lambda\nu)^2}]\right\}. \quad (17)$$

Comparing this equation with Eq. 14, the angular spectrum method actually has the same format with the convolution approach, though they are derived from different models for describing the wave propagation. Within the scope of this paper, the term of "convolution approach" represents these two methods.

Since there is only one (inverse) Fourier transform in the Fresnel and Fraunhofer approximations (see Eqs. 7 and 10), while two (inverse) Fourier transforms are used in the convolution approach (see Eqs. 14 and 17, the former two methods are expected to faster. However, they have to be used in certain conditions of large recording distances, and their reconstruction resolution shrinks with distances increasing [33]. While the convolution approach does not take any approximation, and the reconstruction resolution is equal to the resolution in the hologram. These conclusions can be seen in Fig. 2, which shows the reconstruction results of a copepod hologram using the described methods. The resolution in (b) and (c) shrinks. Shape distortion also occurs in (b) which is caused by the non-square hologram. The hologram cannot be reconstructed using the Fraunhofer approximation, since the reconstruction distance of 61.5 mm does not fulfil the Fraunhofer condition. Overall, the convolution approach performs the best.

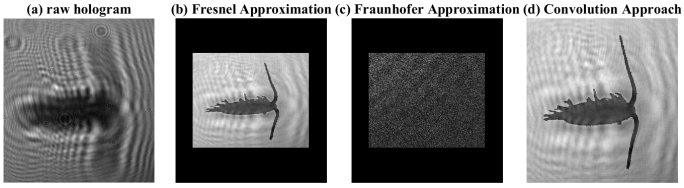

Fig. 2. Reconstruction of a copepod hologram at 61.5 mm using the described methods. (a) raw copepod hologram; (b) Fresnel approximation; (c) Fraunhofer approximation; (d) convolution approach.

In the below content, the convolution approach is adopted to reconstruct holograms unless there is a specification.

B. Noise suppression

Noise is an unavoidable issue in digital in-line hologram processing. It degrades the desired information in images, such as object edges. As well as some common types of optical noise (such as inconsistent exposure cause by instability of the laser source, background noise caused by dirty spots on optics surfaces, and period noise caused by internal reflection or interference in the optical system), digital holograms contain the following intrinsic noise: speckle (from interference of light scattered by the surface points), DC term (non-diffracted wave) and twin image components (fringes from out-of-focus conjugate images). The first step in a conventional workflow for suppressing the noise of inconsistent exposure is to rescale the grey scale of holograms into 0 to 255. The next step is to suppress background noise, period noise, speckle and DC term, where one solution is to subtract a created 'background' image from the rescaled holograms, and another is to remove some low frequencies from its Fourier domain. Two methods are commonly used to create a background image: (1) average intensity of all pixels in the hologram (into a single value) and (2) average intensity of the corresponding pixels of a stack of holograms (into an array). Fig. 3 shows the resultant outputs of the three methods on the copepod hologram in Fig. 2-(a). The reconstruction without noise suppression contains much noise, particularly the DC term, as shown in Fig. 3-(a). Using the average intensity of one hologram can remove some of the DC term (see (b)). The methods of averaging a stack of holograms and removing some low frequencies work better on noise suppression, as shown in (c) and (d). However, none of these methods mitigate the twin image components

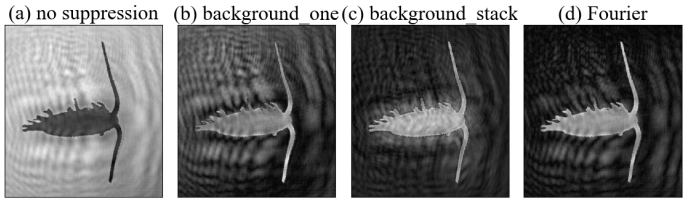

Fig. 3. 3 Results of noise suppression using three common methods when reconstructing the hologram in Fig. 2-(a). (a) reconstruction without noise suppression; (b) reconstruction using the average intensity of the hologram; (c) reconstruction using the average intensity of a stack of 100 holograms which were recorded before the hologram; (d) reconstruction after removing some low Fourier frequencies.

C. Auto-focusing

The hologram of an object can be reconstructed using a reconstruction algorithm when the scattered wave propagates to the plane where the object is recorded. However, the distance of this plane is unknown prior to reconstruction in in situ measurement. A classical solution is to reconstruct the hologram into many slices across the entire recording distance range with a given step, and an image quality metric is then used to seek for the focused reconstruction of the recorded object. This process is called auto-focusing. Many image focus metrics [34,35] can be used to reach this, which depend on an assumption that the focused image contains higher contrast (e.g. edges) than out-of-focus images. Seven widely-used metrics are given in this paper, as listed in TABLE II. The first three metrics are based on intensity statistics, the following two are derived based on intensity histogram, and the last two measure the local gradients across the entire image. These seven metrics were used to predict the focused distance of the raw copepod hologram in Fig. 2-(a), and their resultant curves are depicted in Fig. 4. The hologram was reconstructed between [50, 70] mm with steps of 0.5 mm, and the metrics were computed on the intensity of reconstructed holograms. Please note that the resultant outputs on the phase

reconstruction might change due to phase aberrations [35,36]. All metrics work well on predicting the focus of the hologram, though the result from Tenengrad is slightly different from the others. Empirically speaking, the gradient-based metrics generally work the best, and the histogram-based metrics work better than the statistics-based metrics.

TABLE II
SEVEN FOCUS METRICS AND THEIR EQUATIONS AND INDICATING VALUES OF FOCUS

Integral	$F = \frac{1}{\mathrm{MN}}\sum_{m,n} I(m,n)$
Variance	$F = \frac{1}{\mathrm{MN}}\sum_{m,n}[I(m,n) - \bar{I}]^2$ *
Correlation	$F = \frac{1}{\mathrm{MN}}\lvert\sum_{m,n} I(m,n)^2 - \sum_{m,n} I(m,n)I(m+1,n+1)\rvert$
Energy	$F = \sum_{k=0}^{255} p_k^2$ **
Entropy	$F = -\sum_{k=0}^{255} p_k log_2 p_k$
Brenner	$F = \frac{1}{\mathrm{MN}}\sum_{m,n}[I(m+2,n) - I(m,n)]^2$
Tenengrad	$F = \frac{1}{\mathrm{MN}}\sum_{m,n}[I(m,n) * S_x]^2 + [I(m,n) * S_y]^2$ ***

* I is the image average value.
** p_k is the probability associated with grey level k.
*** S_x and S_y are the Sobel operators.

IV. SUBSEA HOLOCAMERAS

In this section, four subsea digital holocameras that we used or developed in our research projects are introduced. Some parameters of them have been given in TABLE I. Their corresponding software for processing collected holograms is also mentioned here.

A. eHoloCam

eHoloCam, as shown in Fig. 5-(a), was first reported in 2007 [9], and it was developed at the University of Aberdeen (UK). This system has a large recording volume of 36.5 mL. A 4-ns pulsed laser is used such that it is capable of recording fast-moving marine plankton. This camera and its variations have been deployed on numerous research expeditions in the North Sea (Scotland, UK), unobtrusively recording several hundred holographic videos of marine particles and plankton in their natural habitats. HoloCruncher [37], as shown in (b) was developed using C/C++ to process these videos. The convolution approach was used as the reconstruction algorithm, and Tenengrad was used as the focus metric in the software. No noise suppression method was used. It can automatically scan and track the focused reconstructions of recorded objects. The regions of the focused particles, and some morphological features of them (such as size and contours) can also be output, as shown in (c).

B. RamaCam

A concept was recently proposed [38] where DH and Raman spectroscopy were combined into a single system such that it can record the morphological and chemical features of marine particles at the same time. An on-board prototype of this concept, named RamaCam as shown in Fig. 6-(a), was developed in Japan [1]. An in situ version has been tested. This paper only introduces the holocamera of this device. The camera uses a continuous-wave laser to reduce the system size, and an advanced image sensor with short exposure time (7 us at shortest) and fast shutters enables the camera to image moving particles without blur [39]. The camera was tested in the Sagami Bay and Suruga Bay, Japan in 2020, and many holograms were collected. A software package (see (b)) was developed to process recorded holograms. This software is actually a Python-version of HoloCruncher. (c) shows some extracted particles recorded on the cruise.

Due to the specific design of a long flow measurement tube, this camera allows long-scale measurement of the vertical motions and velocities of moving particles. The 3D motion of a copepod in the tube is depicted in Fig. 7 [39].

[1]This was a joint project amongst JAMSTEC (Japan), the University of Tokyo (Japan), the University of Southampton (UK), and the Univesity of Aberdeen (UK)

C. weeHoloCam

In 2021, the University of Aberdeen (UK) developed a state-of-the-art holocamera, named weeHoloCam [30], as shown in Fig. 8-(a). A key feature of this system is its very compact size: at just 9 cm in diameter, 60 cm long, and weighing 3.5 kg. To our knowledge, it is the most compact holocamera so far. It can still record a 12.1 mL water volume per hologram, at up to 25 holograms per second. This camera has been deployed in the North Sea several times, and each time about 200,000 holograms have been recorded. FastScan [30] as shown in (b), the software developed to process recorded holograms, demonstrates the highest processing speed to date. It realises near real-time data processing (˜1 s to extract particles from a 5 MB hologram at 200 planes) via re-interpreting the algorithms in HoloCruncher and running them on a single Field Programmable Gate Array (FPGA). (c) shows some output particles recorded at sea.

D. LISST-HOLO

LISST-HOLO is the first commercial submersible digital holographic camera in the world. The system was developed at the University of Plymouth (UK) [23], and Sequoia (US) [31] holds a world-wide licence for manufacture. The latest version is LISST-HOLO2 (see Fig. 9-(a)). LISST-HOLO has been used by many oceanographic researchers to measure large and complex flocs and biological particles around the world. Sequoia also provides corresponding software – HoloBatch (see (b)) to process recorded holograms. The convolution approach and maximum intensity (Integral) were used to reconstruct and autofocus particles in holograms along with stacked-background subtraction. As well as outputting particle vignettes (see (c) [40]), some particle statistics can also be obtained, such as size distribution.

An embedded CTD (conductivity, temperature, and depth) sensor enables the camera to profile vertical characteristics of marine particles within 600 m depth. Fig. 10 describes some vertical characteristics of a profile recorded using LISSIT-HOLO near South Georgia by Giering et al. in 2017 [40].

V. CONCLUSIONS AND DISCUSSION

Due to high-resolution recording, large depth-of-field and recording volume, and 3D tracking, holography is a powerful

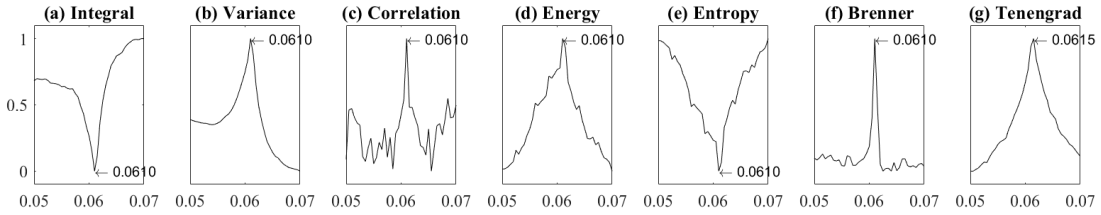

Fig. 4. Curves obtained from the seven metrics on the copepod hologram in Fig. 2-(a), and the value in each plot indicates the predicted focus of the hologram using the corresponding metric.

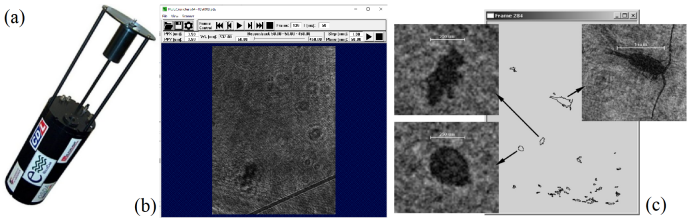

Fig. 5. eHoloCam (a), data processing software – HoloCruncher (b), and a processed frame (hologam) (c).

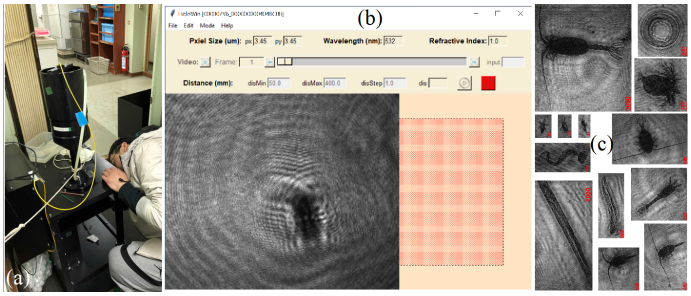

Fig. 6. A prototype of RamaCam (a), data processing software (b), and some output particles (c).

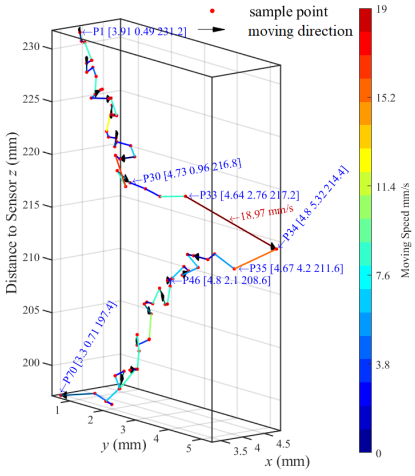

Fig. 7. 3D swimming motion of a copepod in the tube. The red dots correspond to its positions sampled every 0.2 s. The arrows indicate its swimming directions. The coordinates in blue show some sampling points. The colormap describes the average speed between two sampled points. Reconstructed holograms of the copepod at five time points: (a) – P30; (b) – P33; (c) – P34; (d) – P35; and (e) – P46.

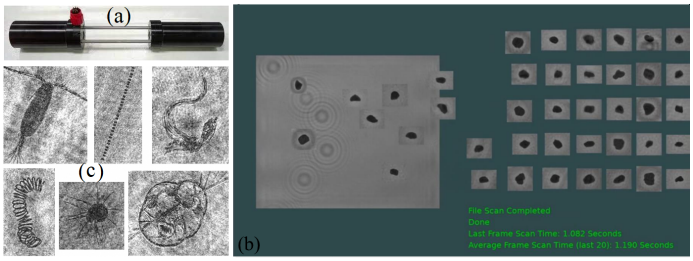

Fig. 8. weeHoloCam (a), data processing software – FastScan (b), and some output particles (c).

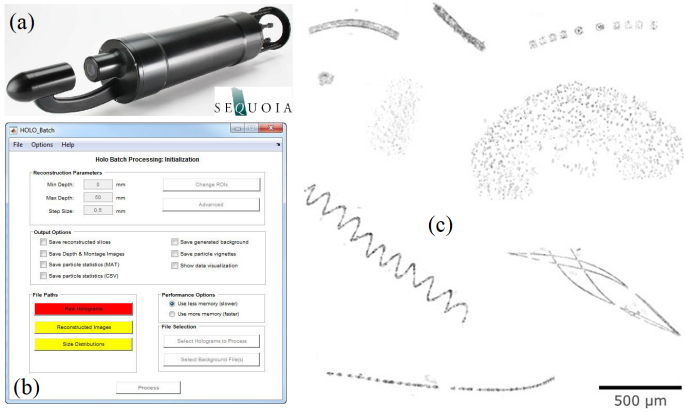

Fig. 9. LISST-HOLO2 (a), data processing software – HoloBatch (b), and some recorded particles in the South Georgia and Benguela current (c).

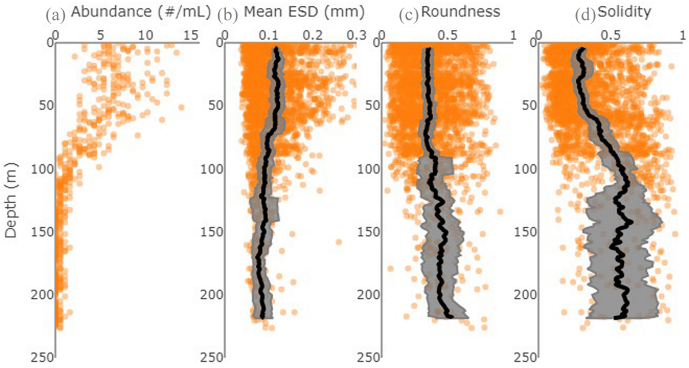

Fig. 10. Vertical characteristics of a profile recorded near South Georgia. (a) number of particles (per mL calculated foreach image); (b) particle ESD (in mm); (c) roundness; (d) solidity. Black lines show running mean (n = 11) for 1-m binned data. Grey envelopes show the corresponding standard deviation.

tool to image microscale objects. It has been used to investigate marine particles and plankton in the laboratory or at sea since 1966. Some classical holocameras were developed to carry out in situ measurement of marine particles and plankton. A milestone came when Owen et al. built a digital holographic setup to monitor marine plankton in 2000. Thereafter, many compact subsea DH cameras were developed. This paper described some common methods to process in-line holograms recorded with the plane wave. Overall, the convolution approach is the best solution to reconstruct this type of hologram. Regarding noise suppression, stacked-background subtraction and removal of low frequencies from holograms work well. The gradient-based metrics generally give reliable predictions for focusing reconstruction. Four subsea digital holocameras were also introduced in this paper. Their success in imaging/measuring marine microscale particles and plankton has evidenced that DH is a promising and powerful imaging technique in marine science.

There are many benefits of using a holocamera to image oceanic microscale objects. However, some limitations also exist:

(1) Monochromatic imaging. Concerning system complexity and underwater colour distortion, most in situ holocameras use a single-wavelength laser and record monochromatic images. This results in losing the colour features of particles in images, which are important to distinguish some marine species (such as jellyfish). A three-wavelength light source (red, green and blue) can be used to image colourful holograms, though this requires a fine optical arrangement and achromatic lens. Regarding software, many AI-based models have been developed to correct underwater image colours.

(2) Much noise. As well as common optical noise, digital in-line holograms contain much intrinsic noise: speckle, DC term and twin image components. They cause problems in extracting accurate morphological properties of imaged particles from holograms, though many traditional methods have been developed to suppress noise (see Hologram Processing-Noise suppression). Machine learning (e.g. denoise autoencoders) provides a new path to address this issue.

(3) Time-consuming reconstruction. Another challenge in DH is the time-consuming processing of reconstruction. For example, a 2 MB hologram takes the order of a minute to be reconstructed in a path of 200 mm with steps of 1 mm. This significantly limits the real-time holographic data processing. However, reconstruction hardware developed for weeHoloCam has shown that FPGAs can be leveraged to accelerate this process by several orders of magnitude. Other researchers are convinced that machine learning is also a solution for this issue.

ACKNOWLEDGMENT

This work is funded by an European research program (Advancing Novel Imaging Technologies and Data Analyses in order to Understand Interior Ocean Carbon Storage (abbreviated as ANTICS), under project code P11105-01).

REFERENCES

[1] Essential Ocean Variables recognised by the Global Ocean Observing System, https://www.goosocean.org/index.php?option=com_content&view=article&layout=edit&id=283&Itemid=441, visited on Dec 11, 2022.

[2] 'How much oxygen comes from the ocean?', National Oceanic and Atmospheric Administration, https://oceanservice.noaa.gov/facts/ocean-oxygen.html, visited on Dec 11, 2022.

[3] Giering, S., et al., Nature 507, 480-483 (2014).

[4] Araujo, G. S., et al., "Plankton: Environmental and Economic Importance for a Sustainable Future", Plankton Communities, edited by Pereira L. and Gonçalves, A. M. M, IntechOpen, 2022, Ch. 2,19-39.

[5] CIPICS, Coastal Ocean Vision, https://coastaloceanvision.com/cpics/, visited on Dec 16, 2022.

[6] Bi, H., et al., "Deployment of an imaging system to investigate fine-scale spatial distribution of early life stages of the ctenophore Mnemiopsis leidyi in Chesapeake Bay", J. Plankton Res 35(2): 270-280 (2013).

[7] Picheral, M., et al., "The Underwater Vision Profiler 6: an imaging sensor of particle size spectra and plankton, for autonomous and cabled platforms", Limnol. Oceanogr.: Methods 20, 115–129 (2022).

[8] Jericho, S. K., et al., "Submersible digital in-line holographic microscope", Rev. Sci. Instrum. 77:043706 (2006).

[9] Sun, H., et al., "In situ underwater electronic holographic camera for studies of plankton", IEEE J. Ocean. Eng. 32(2): 373-382 (2007).

[10] Gabor, D., "A new microscopic principle", Nature 161 (4098): 777–778 (1948).

[11] Knox, C., "Holographic microscopy as a technique for recording dynamic microscopic subjects", Science 153: 989-990 (1966).

[12] Stewart, G. L., et al., "Application of holographic techniques to the study of marine plankton in the field and in the laboratory," Proceedings of the SPIE 41: 183-188 (1974).

[13] Heflinger, L., et al., "Holographic motion pictures of microscopic plankton", Appl. Opt. 17: 951–954 (1978).

[14] Carder, K. L., "In situ holographic measurements of the sizes and settling rates of oceanic particulates", J. Geophys. Res. Oceans 87: 5681–5685 (1982).

[15] Payne, P. R., et al., "Image analysis techniques for holograms of dynamic oceanic particles", Appl. Opt. 23(2): 204-210 (1984).

[16] O'Hern, T., et al., "Comparison of holographic and coulter counter measurements of cavitation nuclei in the ocean", J. Fluids Eng. 110: 200-207 (1988).

[17] Watson, J., et al., "Holographic mensuration of suspended particles in aquatic systems", Proc. SPIE 2577: (1995).

[18] Katz, J., et al., "Submersible holocamera for detection of particle characteristics and motions in the ocean", Deep Sea Res. Part A 46: 1455–1481 (1999).

[19] Watson, J., et al., "Simultaneous in-line and off-axis subsea holographic recording of plankton and other marine particles", Meas. Sci. Technol. 12: L9 (2001).

[20] Owen, R. B., et al., "In-line digital holographic sensor for monitoring and characterizing marine particulates", Opt. Eng. 39: 2187–2197 (2000).

[21] Pfitsch, D., et al., "Development of a free-drifting submersible digital holographic imaging system," in Proceedings of OCEANS 2005MTS/IEEE,Washington, 2005, pp. 690–696.

[22] Jericho, S., et al., "Submersible digital in-line holographic microscope", Rev. Sci. Instrum. 77: 043706 (2006).

[23] Graham, G. W., et al., "The application of holography to the analysis of size and settling velocity of suspended cohesive sediments", Limnol. Oceanogr.: Methods 8(1): 1-15, (2010).

[24] Bochdansky, A. B., et al., "Development and deployment of a point-source digital inline holographic microscope for the study of plankton and particles to a depth of 6000 m", Limnol. Oceanogr.: Methods 11: 28–40 (2013).

[25] Nayak, A. R., et al., "Evidence for ubiquitous preferential particle orientation in representative oceanic shear flows", Limnol. Oceanogr. 63: 122–143 (2018).

[26] Nayak, A. R., et al., "AUTOHOLO: A novel, in situ, autonomous holographic imaging system for long-term particle and plankton characterization studies in diverse marine environments," in Ocean Sciences Meeting 2020, San Diego, US, 2020.

[27] Dyomin, V., et al., “DHC Sensor — a tool for monitoring the plankton biodiversity in a habitat,” OCEANS - MTS/IEEE Kobe, Kobe, Japan, 2018, pp: 1–5.
[28] Dyomin, V., et al., “Underwater holographic sensor for plankton studies in situ including accompanying measurements”, Sensors 21: 4863 (2021).
[29] Dyomin, V., et al., “Study of marine particles using submersible digital holographic camera during the Arctic expedition”, Appl. Sci. 12: 11266 (2022).
[30] Thevar, T., et al., “An ultracompact underwater pulsed digital holographic camera with rapid particle image extraction suite”, IEEE J. Ocean. Eng., In press. JOE Article DOI: 10.1109/JOE.2022.3220880 Manuscript Number: 7951.
[31] LISST-HOLO2, Sequoia Scientific, Inc, https://www.sequoiasci.com/product/lisst-holo/, visited on Dec 17, 2022.
[32] MacNeil, L., et al., “Plankton classification with high-throughput submersible holographic microscopy and transfer learning”, BMC Ecol. Evo. 21:123 (2021).
[33] Schnars, U., et al., “Digital Holography and Wavefront Sensing”, Springer Berlin, Heidelberg, 2015, Ch. 2, 39-68.
[34] Burns, N., et al., “A study of focus metrics and their application to automated focusing of inline transmission holograms”, Imaging Sci. J., 59(2): 90-99 (2011).
[35] İLHAN, H. A., et al., “Digital holographic microscopy and focusing methods based on image sharpness”, J. Microsc., 255(3): 138-149 (2014).
[36] Sirico, D.G., et al., “Compensation of aberrations in holographic microscopes: main strategies and applications”, Appl. Phys. B 128: 78 (2022).
[37] Burns, N., “Robust particle outline extraction and its application to digital in-line holograms of marine organisms”, Opt. Eng. 53(11): 112212 (2014).
[38] Takahashi, T., et al., “Identification of microplastics in a large water volume by integrated holography and Raman spectroscopy”, Appl. Opt. 59(17): 5073-5078 (2020)
[39] Liu, Z., et al., “Digital in-line holography for large-volume analysis of vertical motion of microscale marine plankton and other particles”, IEEE J. Ocean. Eng., 46: 1248-1260 (2021).
[40] Giering, S., et al., “The interpretation of particle size, shape, and carbon flux of marine particle images is strongly affected by the choice of particle detection algorithm”, Front. Mar. Sci. 7: 564 (2020).